Surface & Coatings Technology 393 (2020) 125763

Contents lists available at ScienceDirect

Surface & Coatings Technology

journal homepage: www.elsevier.com/locate/surfcoat

Reactively sputtered TiN/SiO_2 multilayer coatings with designed anisotropic thermal conductivity – From theoretical conceptualization to experimental validation

Michael Tkadletz[a,*], Alexandra Lechner[a], Nina Schalk[a,b], Bernhard Sartory[c], Markus Winkler[d], Christian Mitterer[a]

[a] Department of Materials Science, Montanuniversität Leoben, Franz Josef-Straße 18, 8700 Leoben, Austria
[b] Christian Doppler Laboratory of Advanced Coated Cutting Tools, Montanuniversität Leoben, Franz Josef-Straße 18, 8700 Leoben, Austria
[c] Materials Center Leoben Forschung GmbH, Roseggerstraße 12, 8700 Leoben, Austria
[d] Department Thermal Energy Converters, Fraunhofer Institute for Physical Measurement Techniques, Heidenhofstraße 8, 79110 Freiburg, Germany

ARTICLE INFO

Keywords:
Unbalanced reactive magnetron sputtering
Coating
Anisotropic thermal conductivity
Time-domain thermoreflectance
TDTR

ABSTRACT

Wear resistant coatings are frequently used for cutting applications due to their high hardness, chemical stability and low thermal conductivity. The low thermal conductivity is generally believed to redirect the heat generated during cutting into the chip, while the heat transfer into the tool is kept low. However, a low isotropic thermal conductivity of the applied coatings consequently causes high lateral thermal gradients close to the heat affected zone. These gradients in turn might cause local degradation of mechanical properties, increased local wear and pronounced local thermal stress. A promising concept for thermal management during cutting is the use of coatings with designed anisotropic thermal conductivity. Thereby, the heat flow into the tool can be still kept low, while heat dissipation within the coating can be maximized. Following this concept, the focus of this work is the design, deposition and characterization of coatings with tailored anisotropic thermal conductivity. TiN/SiO_2 multilayer coatings with periodicities between ~100 and ~400 nm and different TiN/SiO_2 thickness ratios resulting in theoretical anisotropy factors ranging from ~1.7 to ~4.0 were designed. Subsequently, corresponding coatings were deposited by unbalanced reactive magnetron sputtering to a total thickness of ~12 μm using Ti and Si targets. The multilayers were prepared for cross-sectional measurements of their in-plane and surface measurements of their cross-plane thermal conductivity by time-domain thermoreflectance to successfully verify the predicted anisotropies.

1. Introduction

Hard coatings are frequently applied to increase the lifetime and performance of cutting tools, due to their high hardness, wear resistance and chemical stability [1,2]. In service, these coatings are exposed to harsh environments, which are dominated by high mechanical and thermal loads. During application, temperatures of ~1000 °C, or even higher, might be reached [3,4]. Thus, significant efforts are made to constantly improve the microstructure, architecture and mechanical properties of the used coatings as well as their thermal stability and oxidation resistance [5–7]. Besides that, it is generally believed that the thermal conductivity of the applied coatings significantly influences the overall performance of the used tools, since it predominantly determines the heat dissipation and thus the temperatures occurring at the cutting edge [4,8]. Hard coatings with low thermal conductivity effectively act as thermal barriers and thus redirect the heat flow into the chip. Consequently, the thermal load on the tool is reduced and plastic deformation of the substrate might be impeded or at least delayed [3]. In turn, however, peak temperatures within the coating increase and pronounced thermal gradients are the consequence. Thus, sophisticated design concepts and optimized thermal management within such coating systems are considered as a key parameter to further increase their performance [9]. Up to now, only a few reports on investigation and tailoring of the thermal conductivity of hard coatings can be found, but recently this topic gains increasing interest in research [10–20].

A promising concept, which has been suggested to improve the thermal management in cutting tools during application, is the implementation of coatings with anisotropic thermal conductivity as

* Corresponding author.
E-mail address: michael.tkadletz@unileoben.ac.at (M. Tkadletz).

https://doi.org/10.1016/j.surfcoat.2020.125763
Received 23 January 2020; Received in revised form 3 April 2020; Accepted 9 April 2020
Available online 14 April 2020
0257-8972/

recently proposed by Böttger et al. [21]. The proposed anisotropy can be established for example by multilayer structures consisting of alternating layers with high and low thermal conductivity. As a consequence, the thermal conductivity parallel to the surface (in-plane) is higher than perpendicular to the surface (cross-plane). Thus, the pronounced anisotropy can reduce thermal gradients along the coating, while the heat flow into the substrate is still kept low.

A reasonable material selection for such a concept might aim towards implementation of transition metal nitrides, as they are frequently used as hard coatings for various applications, with TiN being one of the most established representatives [1]. Recently, Daniel et al. [22] have shown that the combination of TiN and SiO_x in a multilayered architecture significantly improves the fracture mechanical properties compared to their individual constituents. This material combination seemed especially promising to us, since TiN and SiO_2 are known to exhibit a pronounced difference in their thermal conductivity which makes them well suited candidates for the deposition of multilayer coatings with anisotropic thermal conductivity [23,24]. Consequently, this work focuses on the design, synthesis and evaluation of TiN/SiO_2 multilayer coatings with tailored anisotropic thermal conductivity. Following a careful optimization of sample preparation, a multilayer series with different in- and cross-plane thermal conductivities was designed, synthesized and consequently investigated using time-domain thermoreflectance (TDTR).

2. Theoretical conceptualization

A schematic of the correlation between in- and cross-plane thermal conductivity and their effect on the resulting anisotropy is shown in Fig. 1. The dashed line indicates a linear increase with a slope of 1, representing purely isotropic behavior. Below the line, the in-plane thermal conductivity is lower than the cross-plane thermal conductivity, which is defined by an anisotropy factor lower than 1. Such an anisotropy would provide heat flow into the substrate, while the heat dissipation along the coating would be limited. For cutting tools, however, a contrary anisotropy is assumed to be beneficial since in this case, heat diffusion along the lateral direction could help to dissipate energy, reduce peak temperatures and dilute thermal gradients along the coating [21]. This is where an anisotropy with an in-plane to cross-plane ratio higher than 1 comes into play, as it maintains a significantly higher in- than cross-plane thermal conductivity. Fortunately, such anisotropies can be rather easily obtained using available coating deposition equipment, as the most obvious concept for such coatings is based on the deposition of multilayers with a significant difference in the thermal conductivity of their sublayers [21,25,26].

Recently, Böttger et al. suggested a thermal resistor model to predict

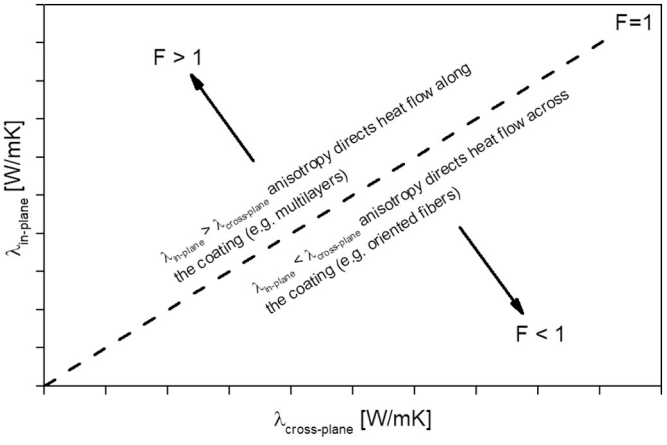

Fig. 1. Schematic illustration of in-plane and cross-plane thermal conductivity and resulting anisotropy.

the anisotropy of periodic multilayer structures, which is applicable to any system containing two species of periodic alternating layers [21]. Within the model, the thicknesses of the two individual sublayers and their corresponding thermal conductivities are considered. If the model is set as independent of the absolute thickness and the interface resistance between the individual layers is neglected, the in- and the cross-plane thermal conductivities $\lambda_{in-plane}$ and $\lambda_{cross-plane}$ can be solely defined by the following equations, where a is the ratio of the thickness of layer 1 and 2 while b is the ratio of their thermal conductivities (λ_1 and λ_2):

$$\lambda_{in-plane} = \lambda_2 \frac{(1+ab)}{1+a} \text{ and } \lambda_{cross-plane} = \lambda_2 \frac{b(1+a)}{a+b} \quad (1)$$

Consequently, the anisotropy factor of the thermal conductivity can be calculated as the ratio of the in- and cross-plane thermal conductivities:

$$F = \frac{\lambda_{in-plane}}{\lambda_{cross-plane}} \text{ resulting in } F = \frac{(a+b)(1+ab)}{b(1+a)^2} \quad (2)$$

Both equations indicate that the in- and cross-plane thermal conductivity and consequently also the anisotropy factor only depend on the thermal conductivity and the thickness of the individual sublayers. Contour plots for a typical parameter range of thermal conductivity [23,24] and layer thicknesses (covering layer thickness ratios a between 1 and 20) within the multilayer system TiN/SiO_2 are shown Fig. 2 for the relative in-plane (a) and cross-plane (b) thermal conductivity as well as for the corresponding anisotropy factor (c). The contour plots show that basically a high relative in-plane thermal conductivity is mainly determined by a large difference in the thermal conductivity of the combined sublayers. The relative cross-plane thermal conductivity shows the highest values for high thermal conductivity ratios in combination with high sublayer thickness ratios. For maximization of the anisotropy, where the relative in-plane thermal conductivity should be as high as possible, while the relative cross-plane thermal conductivity should be as low as possible, the corresponding contour plot indicates that relatively high thermal conductivity ratios should be preferred, while the layer thickness ratio should be kept close to 1. In general, the ratio of the thermal conductivities for a given multilayer system is predetermined by the choice of the corresponding sublayer materials. For the combination of TiN and SiO_2 being within the focus of this work, the b ratio is in the range of ~13.9 [23,24]. Consequently, according to Fig. 2c the anisotropy of TiN/SiO_2 multilayers can be adapted within a range from ~1 to ~4, exclusively depending on the realized sublayer thickness ratio a.

A theoretical parameter variation based on the contour plots presented in Fig. 1 for a TiN/SiO_2 multilayer series with different anisotropies is summarized in Table 1. The sublayer thickness ratio was varied from 1 to 16 and the in- and cross-plane thermal conductivities and their corresponding anisotropy were calculated using the thermal resistor model described above. Subsequently, within the course of this work, the proposed multilayer series as shown in Table 1 has been synthesized.

3. Experimental methods

All coatings investigated within this work have been synthesized by reactive unbalanced magnetron sputtering using a lab scale AJA International ATC-1800 UHV sputtering system. Ar was used as working and N_2 and O_2 as reactive gases. The four magnetrons were equipped with two Si and two Ti targets (diameter 75 mm each). Mirror-polished austenitic stainless steel platelets with a size of $12 \times 6 \times 1$ mm^3 were used as substrates. Prior to the depositions, the substrates were ultrasonically cleaned in acetone and ethanol for 5 min each. After evacuation to a base pressure of $\leq 1 \times 10^{-7}$ mbar, the substrates were heated to the deposition temperature of 400 °C and an etching process using an Ar^+ plasma at a pressure of 5×10^{-3} mbar

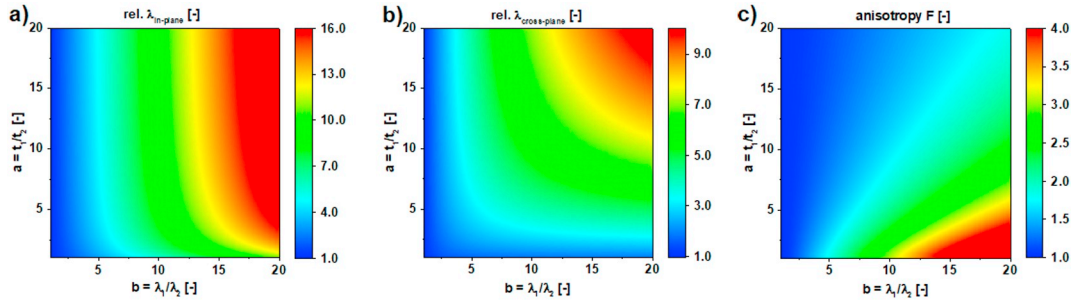

Fig. 2. Contour plots indicating the influence of layer thickness ratio a and thermal conductivity ratio b of TiN/SiO_2 multilayer coatings on relative (a) in-plane thermal conductivity, (b) cross-plane thermal conductivity and (c) resulting relative anisotropy.

was performed to remove remaining surface contaminants. After etching, a ~200 nm Ti adhesion layer was deposited followed by the deposition of the different TiN/SiO_2 multilayers, aiming for a total thickness of ~12 μm. The rather high thickness was necessary for successful in-plane TDTR measurements. During deposition, the total pressure was set to 2×10^{-3} mbar for the synthesis of the TiN layers and 5×10^{-3} mbar for the SiO_2 layers. Thereby, the gas flows were set to 20 sccm for Ar and depending on the individual layer to 5 sccm O_2 or N_2, respectively. The Ti targets were sputtered in DC mode applying a power of 400 W while the Si targets were sputtered in asymmetric bipolar pulsed DC mode at a frequency of 100 kHz and a pulse duration of 1 μs, using a power of 300 W. The applied RF substrate bias power was set to 15 W. Six individual multilayer coatings, as proposed in Table 1, were deposited. The aimed sublayer thickness of the respective multilayer systems was approximated from determined deposition rates of respective single layer sample runs. In addition, a single layer TiN reference coating with a total thickness of 0.9 μm and a single layer SiO_2 reference coating with similar total thickness as the multilayer samples, using the deposition parameters for SiO_2 and TiN as stated above, were grown.

For documentation and basic microstructural characterization, a Zeiss Auriga 40 Crossbeam scanning electron microscope (SEM) and a Zeiss Gemini SEM 450 were used. In order to detect possible Ar^+ ion implantation into the Si and sapphire reference samples during ion slicing and to consider effects of the elemental composition of the TiN and SiO_2 reference coatings on their thermal conductivity, energy dispersive X-ray spectroscopy (EDS) investigations were carried out using an Oxford Instruments Ultim Extreme windowless SDD detector installed on the Gemini SEM 450. Information about the crystallographic structure, phase composition and microstructure of the investigated coatings was obtained via asymmetric X-ray diffraction (XRD) using a Bruker D8 Advance diffractometer. A parallel-beam configuration was used to perform detector scans in a 2θ range of 10–80° at a primary incidence angle θ of 5° and a step size of 0.02°, counting for 1.2 s per step.

Prior to the TDTR measurements, all samples were coated with a pure Al transducer layer [27,28] with a nominal thickness of ~70 nm. The deposition was carried out at room temperature by electron-beam physical vapor deposition using a Leybold LQ560 deposition system. The electrical conductivity of the Al layers was measured by the van der Pauw method, yielding a thermal conductivity of ~200 W/mK using the Wiedemann-Franz law. This is close to the value of bulk Al, indicating good quality and purity of the layers.

For the TDTR measurements, the stainless steel substrates were cut in half to a size of $6 \times 6 \times 1$ mm^3 using a Struers Accutom 50 precision cutting machine. Subsequently, one half of each multilayer sample was used for the cross-plane TDTR measurements for which no special preparation procedure was applied. The other half was used for in-plane TDTR measurements. For successful measurements, smooth and plain coating cross-sections without any edge rounding or break-outs are crucial. Thus, the in-plane samples were prepared by cross-sectional broad Ar^+ ion beam polishing (ion slicing) at, using a Hitachi IM4000+ ion milling system, operated at an accelerating voltage of 6 kV. In addition, to investigate the influence of the cross-sectional preparation procedure on the results of the TDTR measurements, two reference samples (single crystalline Si, p-doped, 100 oriented and single crystalline sapphire, 0001 oriented, both provided by CrysTec [29]) were prepared in same manner. Further, the single layer SiO_2 coating was prepared and measured analogously to the multilayer samples to evaluate the concept and validity of in-plane TDTR measurements.

Subsequently, the TDTR measurements were performed using a pulsed laser pump-probe system, as described in refs. [30, 31]. The necessary laser pulses were generated by the Ti:Sapphire laser system Mai Tai from Spectra-Physics with a pulse width of 500 fs, a pulse repetition rate of 80 MHz, and a wavelength of 785 nm. In order to obtain a representative average thermal conductivity of the system, a sufficiently high thermal penetration and thus information depth for the measurements in cross-plane direction was crucial. Thus, to probe several alternating layers of the multilayer systems during the cross-plane measurements, which were performed on the sample surfaces, the modulation frequency of the pump beam was set to a relatively low frequency of 1.2 MHz. The total average laser beam power (pump plus probe beam) was set to 15 mW with a beam diameter (i.e. $1/e^2$ width) of ~9 μm (central section within the Gaussian intensity profile, where the intensity is above $1/e^2 = 0.135$ times the maximum value). For TDTR measurements, the thermal penetration depth d_t can be estimated for a given modulation frequency f by Eq. (3), if the thermal diffusivity

Table 1
Theoretical parameter variation of TiN/SiO_2 multilayers and corresponding predicted in-plane and cross-plane thermal conductivities as well as their resulting anisotropy based on thermal conductivities of 19.2 W/mK for TiN 1.38 W/mK and SiO_2 taken from refs. [23, 24].

Nomenclature	TiN layer thickness t_1 [nm]	SiO_2 layer thickness t_2 [nm]	Theoretical $a = t_1/t_2$ [−]	Theoretical $b = \lambda_1/\lambda_2$ [−]	Predicted $\lambda_{in-plane}$ [W/mK]	Predicted $\lambda_{cross-plane}$ [W/mK]	Predicted anisotropy F [−]
ML 200/200	200	200	1	13.9	10.3	2.6	4.00
ML 100/100	100	100	1	13.9	10.3	2.6	4.00
ML 50/50	50	50	1	13.9	10.3	2.6	4.00
ML 100/25	100	25	4	13.9	15.6	5.4	2.92
ML 100/12.5	100	12.5	8	13.9	17.2	7.9	2.18
ML 100/6.25	100	6.25	16	13.9	18.2	10.9	1.66

of the investigated material is known [31,32]. The corresponding thermal diffusivity D_t can be calculated using Eq. (4), if the thermal conductivity λ, the specific heat capacity c_p and the density ρ of the material are known.

$$d_t = \sqrt{\frac{2D_t}{2\pi f}} \tag{3}$$

and

$$D_t = \frac{\lambda}{\rho c_p} \tag{4}$$

An estimation of the thermal penetration depth for the extreme cases of pure TiN and SiO_2 using thermophysical data from refs. [23,24] yielded average penetration depths of ~1300 nm for TiN and ~475 nm for SiO_2. Since the actual thermal penetration depth of respective multilayer samples is assumed to consequently lie within these boundary values, a sufficient thermal penetration of all multilayer samples was guaranteed by using a modulation frequency of 1.2 MHz. Directly before to the measurements on the samples, the TDTR measurement system was validated with two reference samples, namely a pure Si wafer and an oxidized one.

While for the cross-plane measurements, which were performed on the sample surfaces, no special alignment procedure was necessary, special emphasis had to be laid on the alignment of the in-plane samples, where the measurements were performed on the prepared coating cross-sections. First, the laser beam was moved to the edge (i.e. coating surface) of the prepared cross-section until a part of the beam was cut off and the probe beam signal intensity (as recorded by a photo diode) was clearly changing. Then it was carefully moved back towards the coating until no cut off could be detected. While further moving the laser beam towards the substrate, the recorded TDTR signal, i.e. the ratio of detector voltages V_{in}/V_{out} [see ref. 30] was monitored. When this signal was considerably changing, it was taken as a sign that the beam was already penetrating the substrate. Finally, the laser beam was moved half way back towards the coating surface, which aligned it exactly in between the coating surface and the coating/substrate interface.

In order to obtain sufficiently accurate results, four to five individual measurements on different positions of each sample were done and averaged. The modeling of the obtained measurement data to extract the thermal conductivity was performed using a semi-infinite solid model as described in ref. [31]. In general, as long as the thermal penetration depth is significantly lower than the laser beam diameter, the heat flow can be assumed as one-dimensional and laterally confined, which was the case for the setup used within this work [28,30,32]. Thus, the TDTR measurement provides the thermal conductivity of the sample along the incidence direction of the laser beam. Consequently, it was assumed that this technique can be also applied for in-plane measurements, as already shown within the work of Böttger et al. [21]. In order to verify this assumption, the deposited single layer SiO_2 reference sample was prepared for cross-plane and in-plane reference measurements. SiO_2 was chosen for this purpose as it was expected to yield an amorphous structure and thus intrinsically homogeneous and isotropic properties.

4. Results and discussion

4.1. Influence of ion beam preparation on TDTR measurements

In order to evaluate the influence of the ion beam polishing (i.e. ion slicing) on the results of the cross-sectional TDTR measurements, two single crystalline reference samples, i.e. 0001 oriented sapphire and 100 oriented Si, were ion sliced analogously to the coating samples. A combined image, showing backscattered electron (BS) SEM images of the prepared sapphire (left) and Si (right) is presented in Fig. 3. It provides an overview of the ion sliced areas and pristine regions of the samples. Using the same parameters, the size of the ion sliced region within the Si is significantly larger than in the sapphire and less curtaining can be observed. Nevertheless, since only rather small spots are illuminated by the laser during TDTR measurements, both the size as well as the surface quality and roughness of the ion slices were assumed to be suitable for TDTR measurements. After deposition of the Al transducer layers, TDTR measurements were performed within the ion sliced areas as well as on pristine sample surfaces. Since ion slicing was performed horizontally, i.e. parallel to the polished surface of the single crystalline reference samples, the TDTR measurements yielded the thermal conductivities of the samples along their specified crystal orientation (0001 for sapphire and 100 for Si). The sufficient intensity of the reflected signal (i.e., probe laser beam) evidenced that the surface roughness after preparation was adequate to perform valid measurements. For the sapphire, a thermal conductivity of 35 ± 6 W/mK was determined on the pristine sample surface, while within the ion sliced area a value of 39 ± 4 W/mK was obtained. Both values are in excellent agreement with literature data reporting values between 35 and 39 W/mK for α-Al_2O_3 [23,33]. The Si sample revealed values of 120 ± 30 W/mK and 138 ± 16 W/mK on the pristine and ion sliced surfaces, respectively, which is in good agreement with literature values of ~140 W/mK reported for Si [30,34–36]. For both samples, increased conductivity values are obtained after ion slicing, while the measurement uncertainty is reduced. Especially in the case of Si, a lower deviation from the reference value is observed after the ion beam preparation. From the observed results it can be concluded that, ion slicing does not negatively affect the TDTR measurements and their quantitative evaluation. In order to further evaluate the influence of the ion slicing procedure, which is generally considered as gentle surface treatment, on the single crystalline reference samples, Monte Carlo simulations of 6 keV Ar^+ ions impinging at grazing incidence on sapphire and Si were performed using the software package SRIM [37–39]. The results, which basically reconstruct the situation during cross-sectional ion slicing as soon as the bulk material which initially protrudes the applied aperture is eroded, revealed ion penetration ranges of ~4 nm in Si and ~2 nm in sapphire at ion backscatter fractions of > 82.5%. Consequently, the actual ion penetration ranges are significantly lower than the estimated thermal penetration and thus information depth of the TDTR measurement. In addition, the high fraction of backscattered ions suggests that only minor amounts of Ar^+ are implanted into the sample cross-section during preparation. This is further corroborated by EDS measurements performed on the Si and sapphire sample after ion slicing, using an acceleration voltage of 5 kV, aiming for a preferably small interaction volume of the electron beam with the sample. The performed measurements did not reveal any indications of Ar^+

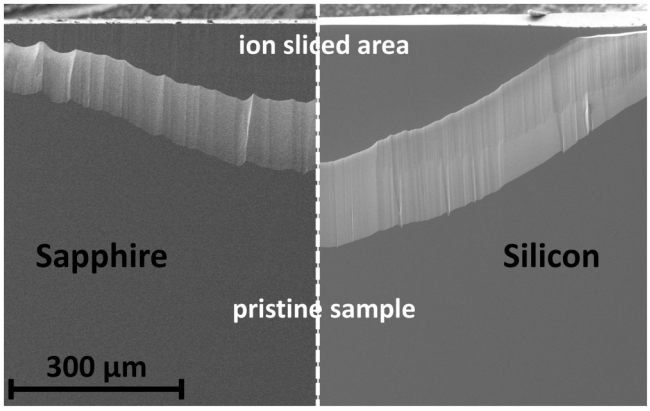

Fig. 3. BS SEM overview of the ion sliced sapphire (left) and Si (right) reference samples, which were used for the verification of the influence of ion beam preparation on TDTR measurements.

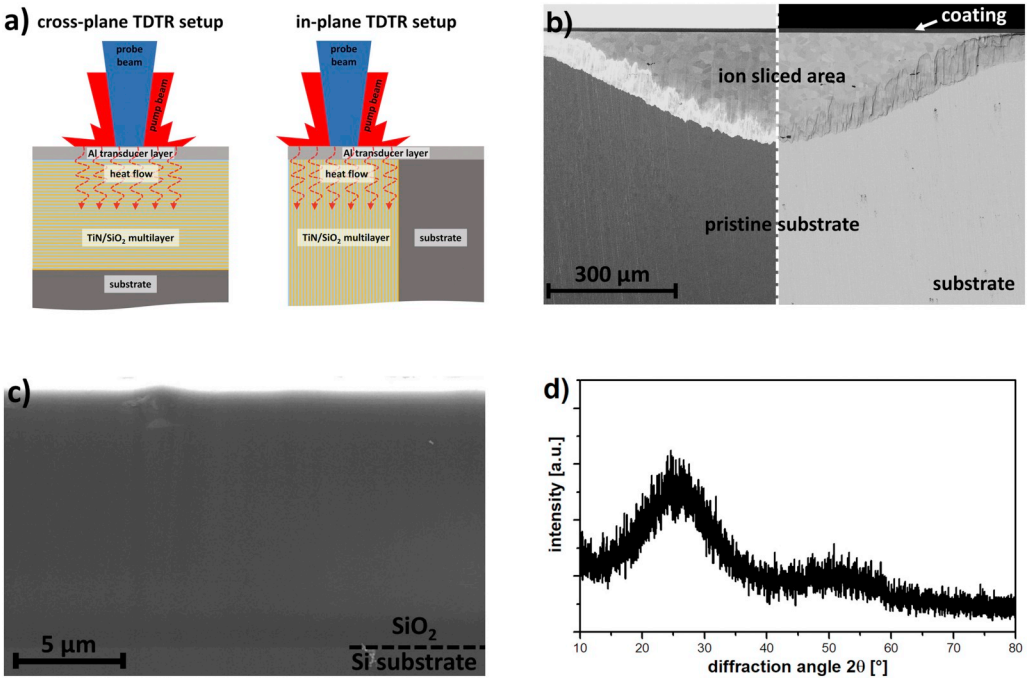

Fig. 4. Schematic illustration of the used cross-plane and in-plane TDTR measurement setup (a) and exemplary SE/BS SEM overview of an ion sliced coating cross-section (100/12.5 TiN/SiO_2 multilayer coating according to Table 1) (b). SE SEM image of the ion sliced cross-section (c) and corresponding X-ray diffractogram (d) of the amorphous SiO_2 coating, which was used to verify the in-plane TDTR measurements.

implantation, neither into the Si nor into the sapphire. Thus, ion beam polishing using Ar^+ ions, seems to be a perfectly suitable method for TDTR. It should be emphasized, however, that this finding cannot be transferred to samples prepared by focused ion beam (FIB) workstations using Ga^+ ions and high acceleration voltages, which are known to alter surface near regions and also implant significant amounts of Ga^+ into the material [40,41].

4.2. Feasibility and validity of cross-sectional in-plane TDTR measurements

Since the measurements on the single crystalline reference samples indicated the feasibility to perform TDTR measurements on ion sliced areas, a series of TiN/SiO_2 multilayer coatings as proposed in Section 2 was deposited for in- and cross- plane TDTR measurements. A sketch of the principal setup of cross-plane and in-plane measurements on an exemplary multilayer sample is shown in Fig. 4a. During cross-plane measurements, both the pump and the probe laser beam are focused on the sample surface. Thus, as long as the sample exhibits a sufficiently low roughness, no special preparation is required. The heat flow during TDTR measurements is generally considered to be one-dimensional for large laser beam dimensions at low thermal penetration depths [28,30,32]. Thus it penetrates the coating across the individual layers of a multilayer sample and the obtained signal yields the cross-plane thermal conductivity. For the in-plane measurements however, a cross-section of the corresponding sample needs to be prepared to allow an alignment of the laser beams along the individual layers, subsequently the in-plane thermal conductivity can be assessed. Fig. 4b shows a combined image of BS and secondary electron (SE) SEM micrographs of an exemplary ion sliced multilayer sample (100/25 TiN/SiO_2, see Table 1) ready for cross-sectional TDTR measurements. Within the ion sliced area, individual grains of the steel substrate can be identified. On top of the ion slice, at the sample edge, the multilayer coating can be clearly seen. Prior to the actual in- and cross-plane TDTR measurements of the multilayer series, a further reference sample, namely a homogeneous single layer SiO_2 coating was deposited onto austenitic steel. Subsequently, the reference coating was prepared for cross-sectional TDTR measurements of its in-plane thermal conductivity as well as for surface TDTR measurements to determine its cross-plane thermal conductivity. Since the coating was expected to be amorphous and intrinsically homogeneous, similar values for the in-plane as well as cross-plane thermal conductivity were expected. A higher magnification SE SEM image of the featureless single layer SiO_2 reference coating is shown in Fig. 4c. The EDS measurements, performed on the as deposited sample prior to the ion slicing procedure, indicated a stoichiometric elemental composition without any other detectable impurities except of ~2 at.% Ar stemming from the sputtering process. The X-ray diffractogram shown in Fig. 4d confirms the amorphous structure of the reference coating. No distinct crystalline peaks can be identified, while the broad peak at ~25° and the slight bump at ~50° indicate the presence of amorphous SiO_2 [42,43]. Thus, no pronounced influence of microstructure or elemental composition on the observed thermal conductivity of the SiO_2 reference coating were expected. The TDTR measurements performed on the surface of the amorphous SiO_2 (i.e., in its cross-plane direction) revealed a thermal conductivity of 1.2 ± 0.2 W/mK, which is close to the literature value of 1.38 W/mK for vitreous silica [23,44]. The in-plane measurements performed on the ion sliced cross-section of the coating yielded a value of 1.3 ± 0.2 W/mK, which is even closer to the literature value, while the difference to the cross-plane measurement is insignificant. Thus it can be concluded that indeed the present sample is intrinsically homogenous in terms of its thermal conductivity. However, even more importantly, the results confirm the feasibility and validity to perform in-plane TDTR measurements in order to determine the cross-plane and in-plane thermal conductivity of multilayered coatings, which is consistent with the previous findings of Böttger et al. [21].

4.3. Microstructure and layer thickness of the TiN/SiO_2 multilayer coatings

SE SEM images of the individual TiN/SiO_2 multilayers, as proposed in Section 2, are summarized in Fig. 5a. Within the images, the TiN layers appear bright, while the SiO_2 layers give dark contrast. For all coatings, the periodic structure can be clearly identified. The SiO_2 sublayer thickness is generally slightly thinner than intended resulting in altered TiN/SiO_2 ratios. In addition, a decreasing regularity of the multilayer structure with decreasing SiO_2 layer thickness can be observed. XRD investigations were performed to analyze the phase composition and microstructural changes with changing sublayer ratio. An exemplary diffractogram of the TiN/SiO_2 100/100 coating is shown in

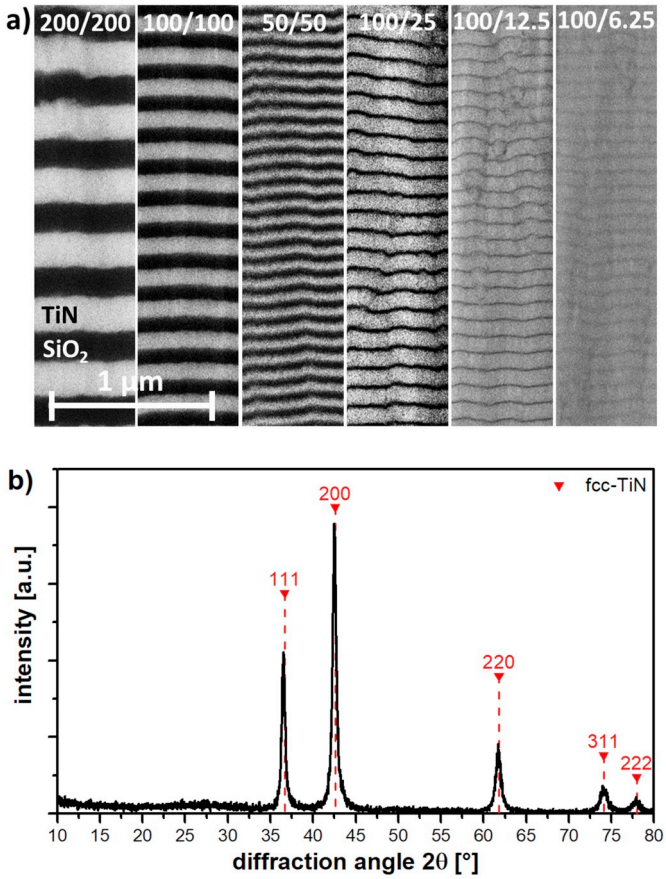

Fig. 5. SE SEM cross-section images of the different TiN/SiO_2 multilayer coatings investigated within this work (see Table 1 for sample denomination) (a). Exemplary X-ray diffractogram of the 100/100 TiN/SiO_2 multilayer coating (b).

Fig. 5b. Characteristic peaks for face-centered cubic TiN according to ICDD card nr. 00–038-1420 are observed. No pronounced preferred orientation of the TiN sublayers can be identified. Again a slight bump in the range between 20° to 35° is visible, which can be assigned to the amorphous SiO_2 sublayers. In general, for the different multilayer coatings, a slightly increasing peak width with decreasing TiN sublayer thickness was observed, which can be attributed to increased size broadening (i.e., smaller domain size). Additionally, with decreasing SiO_2 fraction (i.e., layer thickness) the intensity of the amorphous bump decreased.

Based on the SE SEM images shown in Fig. 5a, the actual sublayer thickness of the individual multilayer coatings was determined and the corresponding sublayer ratio was calculated. Subsequently, the actual in- and cross-plane thermal conductivities as well as the thermal anisotropy were re-estimated using the theoretical thermal conductivity ratio and the thermal resistor model described in Section 2. For the actually deposited multilayer series, the model suggests significantly different in- and cross-plane thermal conductivities, yielding thermal anisotropy factors ranging from ~1.7 to ~4.1. A summary of the investigated samples and their resulting in- and cross-plane thermal conductivities as well as their calculated anisotropy is given in Table 2 and will be discussed in the following section.

4.4. In-plane and cross-plane thermal conductivities

The measured thermal conductivities of the TiN/SiO_2 multilayer coatings in in- and cross-plane direction are presented in Fig. 6a and tabulated in Table 2. The table includes both the measured in-plane and cross-plane thermal conductivity values and thermal anisotropies as well as the estimated values based on Eqs. (1) and (2), for which the layer thicknesses taken from the SEM cross-sections presented in Fig. 5a and thermal conductivities of TiN and SiO_2 reference single layers determined by TDTR were used. For the cross-plane thermal conductivity, a very good agreement of the estimated and measured values is obtained for those coatings with almost equivalent sublayer thickness ratio. This is somewhat unexpected, since the interface spacing in those samples and consequently also the interface density is varying by a factor of 4, which was assumed to have a detectable influence on the measured cross-plane thermal conductivity. Thus, increasing discrepancies of the estimations and measured values were expected for decreasing interface spacing (i.e. sublayer thickness), since the estimations are based on a simplified model omitting the thermal interface resistance. However, as the measurements and the model are in good agreement, it can be assumed that the interface density is still too low to significantly contribute to the cross-plane thermal conductivity of the investigated samples. This is supported by the findings of Costescu et al. [45], who reported on a pronounced influence of the interface resistance on the thermal conductivity of SiO_2 within TiN/SiO_2/Si laminates at a SiO_2 thickness below 25 nm. Samani et al. [12] also observed a decreasing thermal conductivity of TiN/TiAlN multilayer coatings with decreasing sublayer thickness. While no explicit differentiation between microstructural contributions and contributions of increasing interface density is given in their work, again the sublayer thickness exhibiting most pronounced changes was in the range of 6 to 25 nm. Thus it can be concluded, that for multilayer coatings with correspondingly high sublayer thickness, the simplified model yields valid results without the strict necessity of consideration of the thermal interface resistance. For decreasing SiO_2 layer thickness, however, increasing discrepancies from the estimated values tabulated in Table 2 are observed, measured values are considerably higher than estimated values. This can be attributed to the increasing interface softening which is observed with decreasing SiO_2 layer thickness, as obvious from the SE SEM images in Fig. 5a. Consequently, the actual coating architecture increasingly deviates from the model coating architecture presented in Section 2, assuming a strict step-function of the thermal conductivities of the individual sublayers. This mutually yields to deviations of model and measurement in thermal conductivity and accordingly also in the calculated anisotropy. Another possible source for errors is the measurement of the thickness of very thin sublayers, which becomes increasingly challenging with decreasing layer thickness. In contrast, the in-plane thermal conductivity shows in general a good agreement of predictions and measured values. Nevertheless, all samples reveal a slightly lower in-plane thermal conductivity than predicted. This might be an indication for a slightly lower thermal conductivity of the TiN sublayers, in comparison to the tabulated literature value of 19.2 W/mK for bulk TiN [24], which would affect the in-plane thermal conductivity to a greater extent than the cross-plane thermal conductivity. In general, for coatings, a strong influence of deposition conditions and resulting microstructure on the thermal conductivity can be expected [46,47]. For example, Samani et al. reported a value of ~11 ± 1 W/mK for arc evaporated single layer TiN coatings [12] with their inherently high fraction of interfaces due to small crystallite size and microdroplets [25,48,49], while Kainz et al. reported a value as high as 45 W/mK for coarse grained single layer TiN synthesized by chemical vapor deposition [14]. Additionally, the elemental composition of samples is of importance since e.g. impurities, point defects and stoichiometry can have major influence on their thermal conductivity [50]. As seen in Fig. 6a and in Table 2, the in- as well as cross-plane thermal conductivities reach values of ~17 and ~18 W/mK for the multilayer with the lowest SiO_2 sublayer thickness. This suggests that the thermal conductivity of the TiN layers deposited within this work is rather in the range of ~18 W/mK instead of the value of 19.2 W/mK taken from literature, which was used for the initial predictions shown in Table 1. In fact, the TDTR measurements on the single layer TiN reference coating investigated within this work revealed a thermal

Table 2
Actual TiN/SiO_2 multilayers investigated within this work and their estimated and measured in- and cross-plane thermal conductivities as well as their corresponding anisotropy. The estimated values are based on the actually obtained thickness ratio *a* and the actual thermal conductivity ratio *b*, which was determined by TDTR measurements on the single layer TiN and SiO_2 reference coatings.

Nomenclature	TiN layer thickness t_1 [nm]	SiO_2 layer thickness t_2 [nm]	Actual a = t_1/t_2 [−]	Actual b = λ_1/λ_2 [−]	$\lambda_{in-plane}$ [W/mK]		$\lambda_{cross-plane}$ [W/mK]		Anisotropy F [−]	
					Estimated	Measured	Estimated	Measured	Estimated	Measured
ML 200/200	214	170	1.25	14.4	10.6	9.2 ± 1.3	2.6	2.0 ± 0.3	4.08	4.6 ± 1.3
ML 100/100	107	87	1.23	14.4	10.5	10.0 ± 1.0	2.6	2.6 ± 0.3	4.08	3.8 ± 0.8
ML 50/50	60	40	1.5	14.4	11.3	8.9 ± 0.9	2.8	2.5 ± 0.3	3.99	3.6 ± 0.8
ML 100/25	92	20	4.6	14.4	15.0	14.0 ± 1.4	5.3	6.9 ± 0.7	2.83	2.0 ± 0.4
ML 100/12.5	80	10	8	14.4	16.1	16.0 ± 2.0	7.2	10.0 ± 1.0	2.23	1.6 ± 0.4
ML 100/6.25	80	5	16	14.4	17.0	17.0 ± 2.0	10.1	18.0 ± 2.0	1.69	0.9 ± 0.2

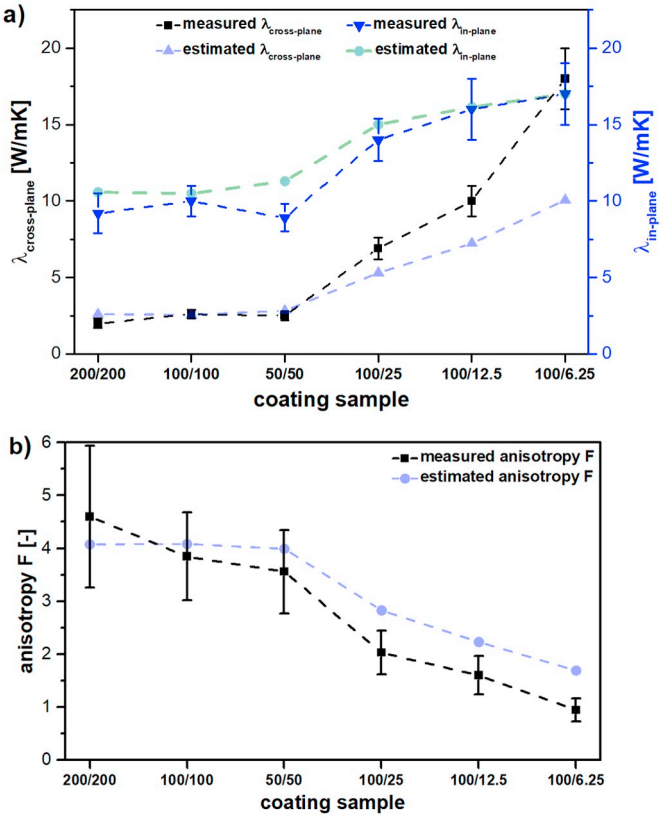

Fig. 6. (a) Measured and estimated in-plane and cross-plane thermal conductivities and (b) calculated anisotropy of the investigated TiN/SiO_2 multilayer coatings. The estimated values are based on the actually obtained thickness ratio *a* and the actual thermal conductivity ratio *b*, which was determined by TDTR measurements on the single layer TiN and SiO_2 reference coatings.

conductivity of 18 ± 2 W/mK. This value seems consistent for all TiN sublayers; no indications for a pronounced dependency of the sublayer thickness on the individual thermal conductivities are found. The slightly lower value compared to the tabulated literature value might be owed to microstructural effects as described above. In addition, the EDS measurements of the as deposited TiN reference coating indicated a slight N deficiency of ~1.8 ± 0.1 at.% which might affect the thermal conductivity to a certain extent. Apart from that, analogously to the SiO_2 sample, no other impurities, except of ~2 at.% Ar stemming from the sputtering process, could be detected. The anisotropy, which was calculated from the measured in- and cross-plane thermal conductivities, is presented in Fig. 6b and Table 2, including error estimates based on error propagation calculations, where again the estimated anisotropy is added as well. A reasonable agreement of estimated and measured anisotropy values is found. The fact that the anisotropy of the 200/200 multilayer coating is the only value which is higher than the estimated anisotropy might be owed to the limited information depth available for the cross-plane measurement. For this particular coating, the thermal penetration depth was in the range of ~1–1.5 layer stacks of TiN and SiO_2, and SiO_2 formed the top-layer. Due to the exponential decay of the thermal signal for an increasing penetration into the sample, the sample information originates mainly from the top layer of the sample. Since SiO_2 has a significantly lower thermal conductivity than TiN, for this particular sample the SiO_2 layer might have affected the measurement disproportionally high. Thus, it is recommended that for future experiments at least several sublayer stacks of multilayer samples should be probed using this technique. The actually lower anisotropy of multilayers with thin SiO_2 sublayers is a direct result of their higher cross-plane thermal conductivity compared to the expected values. This effect could be overcome in future works by putting special emphasis on layer regularity and homogeneity. However, to deposit coatings with low or no anisotropy, multilayered architectures are not necessarily required and thus, this discrepancy is probably negligible. Besides that, the thermal stability as well as mechanical properties of single layer TiN and especially SiO_2 are moderate compared to other hard coatings [1,5,51–53]. Thus, a logical progression within future works, might aim to extend the results of this work to coating systems with higher thermal stability and more favorable mechanical properties. The crucial challenge, however, is to find suitable candidates to combine, which likewise deliver the necessary high contrast in thermal conductivity. Another fact which should be addressed is that during the measurement - due to the continuous laser pulsing - the temperature on the sample rises (so called steady state temperature rise [31,54]). The rise in temperature is inversely proportional to the thermal conductivity of the investigated material, as it directly influences the heat dissipation during the measurement. According to the models proposed in [31,54], for the particular parameters of the TDTR setup used within this work, the rise to steady state temperature for a single layer TiN coating is in the range of ~5–10 °C, while for a single layer SiO_2 coating it is ~120–130 °C. Consequently, the measurements have to be considered to yield the thermal conductivity of the sample at the particular steady state temperatures. While for an isotropic single layer SiO_2 sample, the increase in temperature is the same for in- and cross-plane measurements, that is not the case for anisotropic samples. For the samples investigated within this work, the difference in steady state temperature between in- and cross-plane measurements was estimated to be ~6–63 °C at a total rise of ~10–80 °C. In general, the change in thermal conductivity over temperature for materials similar to those investigated within this study is reported to be small [13,15,20]; thus, for this work the difference in steady state temperature is considered to be not substantial.

5. Conclusions

Within the course of this work, theoretical considerations using a thermal resistor model allowed to conceptualize a series of multilayer coatings with highly anisotropic thermal conductivities, yielding

anisotropy factors from ~1.7 to ~4.0. Accordingly, a series of corresponding TiN/SiO_2 samples was deposited using unbalanced reactive magnetron sputter deposition. The actual layer thicknesses and thermal conductivities of the individual sublayers were fed into the model to estimate the actually expected in-plane and cross-plane thermal conductivities as well as thermal anisotropies. Subsequently, a technique to determine the in-plane thermal conductivity of hard coatings using time-domain thermoreflectance (TDTR) was successfully applied. For this purpose, a carefully optimized ion beam assisted preparation procedure for coating cross-sections and subsequent in-plane TDTR measurements was utilized. Special emphasis was laid on the influence of the sample preparation on the TDTR results and validation of in-plane TDTR measurements. Subsequently, in- and cross-plane TDTR measurements on the multilayer samples were performed. The obtained results revealed good agreement of measurements and model in terms of in- and cross-plane thermal conductivity as well as estimated thermal anisotropies. This work clearly demonstrates that the design and subsequent characterization of coatings with anisotropic thermal conductivity represents a vast playground to improve their thermal performance during application.

CRediT authorship contribution statement

Michael Tkadletz:Conceptualization, Formal analysis, Investigation, Validation, Writing - original draft, Writing - review & editing, Visualization, Project administration.**Alexandra Lechner**: Formal analysis, Investigation, Validation.**Nina Schalk**:Writing - original draft, Writing - review & editing.**Bernhard Sartory**: Investigation, Validation.**Markus Winkler**:Investigation, Validation. **Christian Mitterer**:Writing - original draft, Supervision, Funding acquisition.

Declaration of competing interest

The authors declare that they have no known competing financial interests or personal relationships that could have appeared to influence the work reported in this paper.

Acknowledgements

The authors gratefully acknowledge the financial support under the scope of the COMET program within the K2 Center “Integrated Computational Material, Process and Product Engineering (IC-MPPE)” (Project No 859480). This program is supported by the Austrian Federal Ministries for Transport, Innovation and Technology (BMVIT) and for Digital and Economic Affairs (BMDW), represented by the Austrian research funding association (FFG), and the federal states of Styria, Upper Austria and Tyrol. The financial support by the Austrian Federal Ministry for Digital and Economic Affairs and the National Foundation for Research, Technology and Development is gratefully acknowledged.

References

[1] P.H. Mayrhofer, R. Rachbauer, D. Holec, F. Rovere, J.M. Schneider, Protective transition metal nitride coatings, in: V.K. Sarin, L. Llanes, D. Mari, C.E. Nebel (Eds.), Comprehensive Hard Materials, 4 Elsevier, London, 2014, pp. 355–388.
[2] C. Mitterer, PVD and CVD hard coatings, in: V.K. Sarin, L. Llanes, D. Mari, C.E. Nebel (Eds.), Comprehensive Hard Materials, 2 Elsevier, London, 2014, pp. 449–467.
[3] A.W. Nemetz, W. Daves, T. Klünsner, W. Ecker, T. Teppernegg, C. Czettl, I. Krajinović, FE temperature- and residual stress prediction in milling inserts and correlation with experimentally observed damage mechanisms, J. Mater. Process. Technol. 256 (2018) 98–108.
[4] I. Krajinović, W. Daves, M. Tkadletz, T. Teppernegg, T. Klünsner, N. Schalk, C. Mitterer, C. Tritremmel, W. Ecker, C. Czettl, Finite element study of the influence of hard coatings on hard metal tool loading during milling, Surf. Coat. Technol. 304 (2016) 134–141.
[5] P.H. Mayrhofer, C. Mitterer, L. Hultman, H. Clemens, Microstructural design of hard coatings, Prog. Mater. Sci. 51 (2006) 1032–1114.
[6] B. Grossmann, N. Schalk, C. Czettl, M. Pohler, C. Mitterer, Phase composition and thermal stability of arc evaporated $Ti_{1-x}Al_xN$ hard coatings with $0.4 \leq x \leq 0.67$, Surf. Coat. Technol. 309 (2017) 687–693.
[7] B. Grossmann, M. Tkadletz, N. Schalk, C. Czettl, M. Pohler, C. Mitterer, High-temperature tribology and oxidation of $Ti_{1-x-y}Al_xTa_yN$ hard coatings, Surf. Coat. Technol. 342 (2018) 190–197.
[8] J. Dörr, T. Mertens, G. Engering, M. Lahres, “In-situ” temperature measurement to determine the machining potential of different tool coatings, Surf. Coat. Technol. 174–175 (2003) 389–392.
[9] A.W. Nemetz, W. Daves, T. Klünsner, C. Praetzas, W. Liu, T. Teppernegg, C. Czettl, F. Haas, C. Bölling, J. Schäfer, Experimentally validated calculation of the cutting edge temperature during dry milling of Ti6Al4V, J. Mater. Process. Technol. 278 (2020) 116544.
[10] X.Z. Ding, M.K. Samani, G. Chen, Thermal conductivity of PVD TiAlN films using pulsed photothermal reflectance technique, Appl. Phys. A Mater. Sci. Process. 101 (2010) 573–577.
[11] M.K. Samani, G.C.K. Chen, X.Z. Ding, X.T. Zeng, Thermal conductivity of CrAlN and TiAlN coatings deposited by lateral rotating cathode arc, Key Eng. Mater. 447–448 (2010) 705–709.
[12] M.K. Samani, X.Z. Ding, N. Khosravian, B. Amin-Ahmadi, Y. Yi, G. Chen, E.C. Neyts, A. Bogaerts, B.K. Tay, Thermal conductivity of titanium nitride/titanium aluminum nitride multilayer coatings deposited by lateral rotating cathode arc, Thin Solid Films 578 (2015) 133–138.
[13] G.S. Fox-Rabinovich, K. Yamamoto, M.H. Aguirre, D.G. Cahill, S.C. Veldhuis, A. Biksa, G. Dosbaeva, L.S. Shuster, Multi-functional nano-multilayered AlTiN/Cu PVD coating for machining of Inconel 718 superalloy, Surf. Coat. Technol. 204 (2010) 2465–2471.
[14] C. Kainz, N. Schalk, M. Tkadletz, C. Saringer, M. Winkler, A. Stark, N. Schell, J. Julin, C. Czettl, Thermo-physical properties of coatings in the Ti(B,N) system grown by chemical vapor deposition, Surf. Coat. Technol. 384 (2020) 125318.
[15] W. Kalss, A. Reiter, V. Derflinger, C. Gey, J.L. Endrino, Modern coatings in high performance cutting applications, Int. J. Refract. Met. Hard Mater. 24 (2006) 399–404.
[16] J. Martan, P. Beneš, Thermal properties of cutting tool coatings at high temperatures, Thermochim. Acta 539 (2012) 51–55.
[17] R. Rachbauer, J.J. Gengler, A.A. Voevodin, K. Resch, P.H. Mayrhofer, Temperature driven evolution of thermal, electrical, and optical properties of Ti–Al–N coatings, Acta Mater. 60 (2012) 2091–2096.
[18] M. Tkadletz, N. Schalk, R. Daniel, J. Keckes, C. Czettl, C. Mitterer, Advanced characterization methods for wear resistant hard coatings: a review on recent progress, Surf. Coat. Technol. 285 (2016) 31–46.
[19] H. Chen, B.C. Zheng, Y.X. Ou, M.K. Lei, Microstructure and thermal conductivity of Ti-Al-Si-N nanocomposite coatings deposited by modulated pulsed power magnetron sputtering, Thin Solid Films 693 (2020) 137680.
[20] J. Zhao, Z. Liu, Q. Wang, J. Jiang, Measurement of temperature-dependent thermal conductivity for PVD $Ti_{0.55}Al_{0.45}N$ ceramic coating by time domain thermo-reflectance method, Ceram. Int. 45 (2019) 8123–8129.
[21] P.H.M. Böttger, L. Braginsky, V. Shklover, E. Lewin, J. Patscheider, D.G. Cahill, M. Sobiech, Hard wear-resistant coatings with anisotropic thermal conductivity for high thermal load applications, J. Appl. Phys. 116 (2014) 013507.
[22] R. Daniel, M. Meindlhumer, J. Zalesak, B. Sartory, A. Zeilinger, C. Mitterer, J. Keckes, Fracture toughness enhancement of brittle nanostructured materials by spatial heterogeneity: a micromechanical proof for CrN/Cr and TiN/SiO_x multilayers, Mater. Des. 104 (2016) 227–234.
[23] H. Warlimont, W. Martienssen, Springer Handbook Condensed Matter and Materials Data, Springer Berlin Heidelberg, 2005.
[24] H.O. Pierson, Handbook of Refractory Carbides & Nitrides: Properties, Characteristics, Processing and Apps, Noyes Publications, Westwood, New Jersey, 1996.
[25] P.H.M. Böttger, A.V. Gusarov, V. Shklover, J. Patscheider, M. Sobiech, Anisotropic layered media with microinclusions: thermal properties of arc-evaporation multilayer metal nitrides, Int. J. Therm. Sci. 77 (2014) 75–83.
[26] L. Braginsky, A. Gusarov, V. Shklover, Models of thermal conductivity of multilayer wear resistant coatings, Surf. Coat. Technol. 204 (2009) 629–634.
[27] Y. Wang, J.Y. Park, Y.K. Koh, D.G. Cahill, Thermoreflectance of metal transducers for time-domain thermoreflectance, J. Appl. Phys. 108 (2010) 1–4.
[28] W.S. Capinski, H.J. Maris, T. Ruf, M. Cardona, K. Ploog, D.S. Katzer, Thermal-conductivity measurements of GaAs/AlAs superlattices using a picosecond optical pump-and-probe technique, Phys. Rev. B 59 (1999) 8105–8113.
[29] Crystec.de, CrysTec GmbH. [online], Available at http://crystec.de/crystec-d.html, (2020) , Accessed date: 15 January 2020.
[30] D.G. Cahill, W.K. Ford, K.E. Goodson, G.D. Mahan, A. Majumdar, H.J. Maris, R. Merlin, S.R. Phillpot, Nanoscale thermal transport, J. Appl. Phys. 93 (2003) 793–818.
[31] D.G. Cahill, Analysis of heat flow in layered structures for time-domain thermoreflectance, Rev. Sci. Instrum. 75 (2004) 5119–5122.
[32] X. Qian, P. Jiang, R. Yang, Anisotropic thermal conductivity of 4H and 6H silicon carbide measured using time-domain thermoreflectance, Mater. Today Phys. 3 (2017) 70–75.
[33] D.G. Cahill, S.-M. Lee, T.I. Selinder, Thermal conductivity of κ-Al_2O_3 and α-Al_2O_3 wear-resistant coatings, J. Appl. Phys. 83 (1998) 5783–5786.
[34] M. Asheghi, M.N. Touzelbaev, K.E. Goodson, Y.K. Leung, S.S. Wong, Temperature-dependent thermal conductivity of single-crystal silicon layers in SOI substrates, J. Heat Transf. 120 (1998) 30–36.
[35] D.G. Cahill, K. Goodson, A. Majumdar, Thermometry and thermal transport in micro/nanoscale solid-state devices and structures, J. Heat Transf. 124 (2002)

223–241.
[36] A.J. Schmidt, X. Chen, G. Chen, Pulse accumulation, radial heat conduction, and anisotropic thermal conductivity in pump-probe transient thermoreflectance, Rev. Sci. Instrum. 79 (2008) 114902.
[37] J.F. Ziegler, J.P. Biersack, M.D. Ziegler, SRIM: The Stopping and Range of Ions in Matter, SRIM Co, Chester, Maryland, 2008.
[38] J.F. Ziegler, M.D. Ziegler, J.P. Biersack, SRIM – the stopping and range of ions in matter (2010), Nucl. Instruments Methods Phys. Res. Sect. B Beam Interact. with Mater. Atoms 268 (2010) 1818–1823.
[39] J.P. Biersack, L.G. Haggmark, A Monte Carlo computer program for the transport of energetic ions in amorphous targets, Nucl. Instrum. Methods 174 (1980) 257–269.
[40] Y.J. Xiao, F.Z. Fang, Z.W. Xu, W. Wu, X.C. Shen, The study of Ga^+ FIB implanting crystal silicon and subsequent annealing, Nucl. Instruments Methods Phys. Res. Sect. B Beam Interact. with Mater. Atoms 307 (2013) 253–256.
[41] J. Huang, M. Loeffler, W. Moeller, E. Zschech, Ga contamination in silicon by focused ion beam milling: dynamic model simulation and atom probe tomography experiment, Microelectron. Reliab. 64 (2016) 390–392.
[42] J. Sun, Z. Xu, W. Li, X. Shen, Effect of nano-SiO_2 on the early hydration of alite-sulphoaluminate cement, Nanomaterials 7 (2017) 102.
[43] P. Deshmukh, J. Bhatt, D. Peshwe, S. Pathak, Determination of silica activity index and XRD, SEM and EDS studies of amorphous SiO_2 extracted from rice husk ash, Trans. Indian Inst. Metals 65 (2012) 63–70.
[44] D.G. Cahill, Thermal conductivity measurement from 30 to 750 K: the 3ω method, Rev. Sci. Instrum. 61 (1990) 802–808.
[45] R.M. Costescu, M.A. Wall, D.G. Cahill, Thermal conductance of epitaxial interfaces, Phys. Rev. B 67 (2003) 054302.
[46] Ö. Altun, Y.E. Böke, Effect of the microstructure of EB-PVD thermal barrier coatings on the thermal conductivity and the methods to reduce the thermal conductivity, Arch. Mater. Sci. Eng. 40 (2009) 47–52.
[47] A. Kusiak, J. Martan, J.-L. Battaglia, R. Daniel, Using pulsed and modulated photothermal radiometry to measure the thermal conductivity of thin films, Thermochim. Acta 556 (2013) 1–5.
[48] M. Tkadletz, C. Mitterer, B. Sartory, I. Letofsky-Papst, C. Czettl, C. Michotte, The effect of droplets in arc evaporated TiAlTaN hard coatings on the wear behavior, Surf. Coat. Technol. 257 (2014) 95–101.
[49] M. Pohler, R. Franz, J. Ramm, P. Polcik, C. Mitterer, Cathodic arc deposition of $(Al,Cr)_2O_3$: macroparticles and cathode surface modifications, Surf. Coat. Technol. 206 (2011) 1454–1460.
[50] N. Tureson, M. Marteau, T. Cabioch, N. Van Nong, J. Jensen, J. Lu, G. Greczynski, D. Fournier, N. Singh, A. Soni, L. Belliard, P. Eklund, A. le Febvrier, Effect of ion-implantation-induced defects and Mg dopants on the thermoelectric properties of ScN, Phys. Rev. B 98 (2018) 205307.
[51] U. Beck, D.T. Smith, G. Reiners, S.J. Dapkunas, Mechanical properties of SiO_2 and Si_3N_4 coatings: a BAM/NIST co-operative project, Thin Solid Films 332 (1998) 164–171.
[52] M.D. Michel, F.C. Serbena, C.M. Lepienski, Effect of temperature on hardness and indentation cracking of fused silica, J. Non-Cryst. Solids 352 (2006) 3550–3555.
[53] F. Giuliani, C. Ciurea, V. Bhakhri, M. Werchota, L.J. Vandeperre, P.H. Mayrhofer, Deformation behaviour of TiN and Ti–Al–N coatings at 295 to 573 K, Thin Solid Films 688 (2019) 137363.
[54] M. Winkler, Nanostructured Thermoelectrics: Bi_2Te_3/Sb_2Te_3 Based Superlattice Systems Fabricated by MBE and Sputtering, PhD Thesis Eberhard Karls Univeristät Tübingen, 2014.